Journal Pre-proof

Activation of peroxymonosulfate using carbon black nano-spheres/calcium alginate hydrogel matrix for degradation of acetaminophen: Fe_3O_4 co-immobilization and microbial community response

Reza Darvishi Cheshmeh Soltani, Mansoureh Mahmoudi, Grzegorz Boczkaj, Alireza Khataee

PII: S1226-086X(20)30359-2

DOI: https://doi.org/10.1016/j.jiec.2020.08.006

Reference: JIEC 5174

To appear in: *Journal of Industrial and Engineering Chemistry*

Received Date: 4 June 2020

Revised Date: 1 August 2020

Accepted Date: 1 August 2020

Activation of peroxymonosulfate using carbon black nano-spheres/calcium alginate hydrogel matrix for degradation of acetaminophen: Fe_3O_4 co-immobilization and microbial community response

Reza Darvishi Cheshmeh Soltani,[a,*] Mansoureh Mahmoudi,[a] Grzegorz Boczkaj,[b] Alireza Khataee,[c,d,*]

[a]Department of Environmental Health Engineering, School of Health, Arak University of Medical Sciences, Arak, Iran

[b]Gdansk University of Technology, Faculty of Chemistry, Department of Process Engineering and Chemical Technology, 80-233 Gdansk, G. Narutowicza St. 11/12, Poland

[c]Research Laboratory of Advanced Water and Wastewater Treatment Processes, Department of Applied Chemistry, Faculty of Chemistry, University of Tabriz, 51666-16471 Tabriz, Iran

[d]Institute of Research and Development, Duy Tan University, Da Nang 550000, Vietnam

[*]Corresponding authors: rezadarvish86@yahoo.com (R. Darvishi Cheshmeh Soltani)
a_khataee@tabrizu.ac.ir, alirezakhataee@duytan.edu.vn (A. Khataee)

Graphical abstract

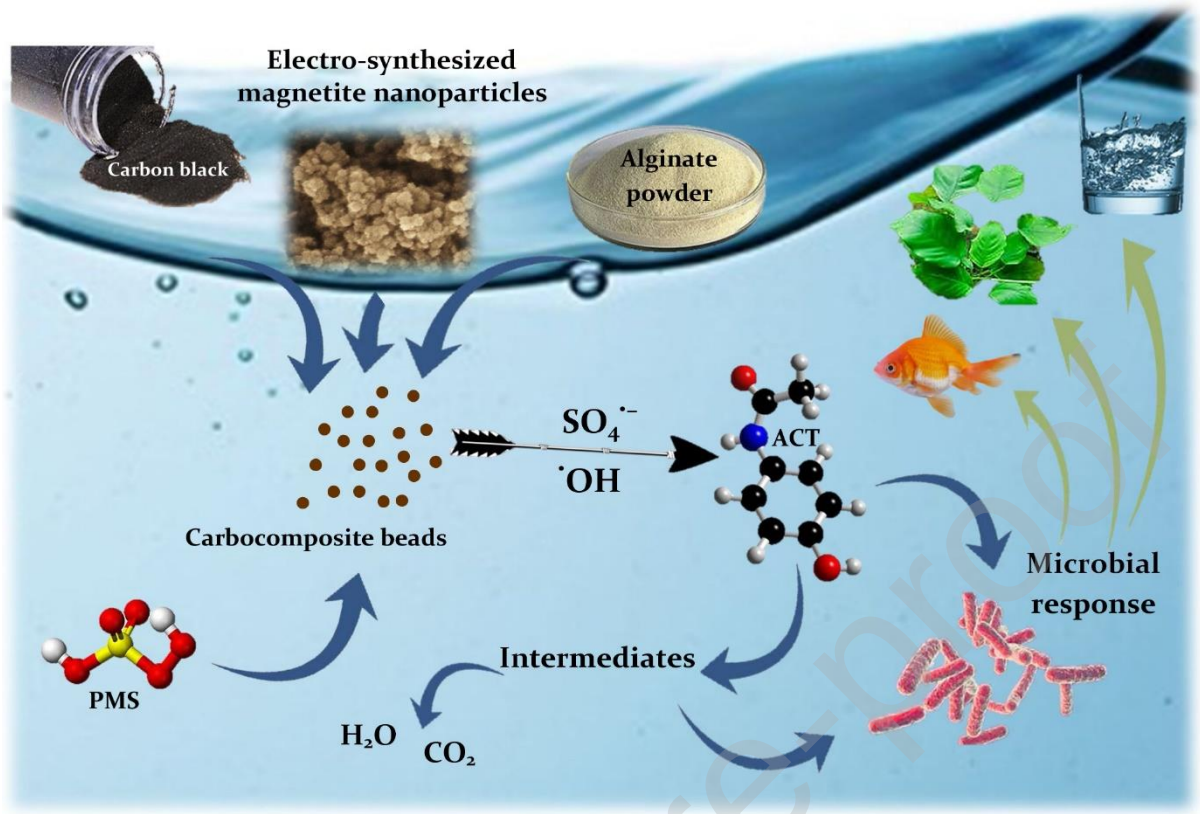

Research highlights

- Integration of carbon black nano-spheres with calcium alginate hydrogel to activate PMS
- Hardness, alkalinity, nutrients and scavengers were considered during the process
- Enhanced efficiency via co-immobilization with nano-sized magnetite
- Evaluation of effluent bio-toxicity by microbial community response

Abstract

Herein, we focused on the degradation of acetaminophen (ACT) drug in liquid phase by peroxymonosulfate (PMS) activated by carbon black nano-spheres (CBNS). The nanostructured

activator was immobilized into calcium alginate hydrogel matrix (CAHM) to avoid the washout of the fine nanostructures. The Langmuir modeling showed an insignificant contribution to the adsorption process in the removal of ACT. The basic pH conditions favored the decomposition of ACT. Among nutrients, the presence of nitrogenous compounds including nitrite, nitrate and ammonium caused a little decrease in the reactor performance, while the addition of phosphate ion improved the efficiency from 76.8 to 81.9%. The results demonstrated the involvement of both $SO_4^{\bullet-}$ and $^{\bullet}OH$ radicals in the degradation of ACT and domination of $SO_4^{\bullet-}$ radicals in the degradation process. Co-immobilization of the CBNS with electro-synthesized magnetite nanoparticles resulted in not only the enhanced reusability potential but also improved the efficiency of the treatment process to 95.6%. Mineralization efficiency of the process was not remarkable; however, the process produced an effluent with lower toxicity toward the microbial community of the activated sludge.

Keywords: Pharmaceuticals; Peroxymonosulfate (PMS); Nano-carbon black; Sodium alginate; Magnetite nanoparticles

1. Introduction

Pharmaceutical compounds have been extensively produced, consumed and discharged into various environments over the past years. They have been detected in the industrial wastewaters and also natural water resources such as lakes and rivers in the range of ng/L to g/L due to their chemical resistance [1, 2]. Among pharmaceuticals, anti-inflammatory and non-narcotic analgesic drugs such as acetaminophen (ACT) are considered as extensively consumed drugs with refractory properties that are inadequately treatable in conventional wastewater treatment

processes [3]. ACT is widely prescribed for the relief of headaches and fever, along with the treatment of flu and cold [3, 4]. However, excessive consumption of ACT can result in kidney and liver damages as a result of being metabolized to N-acetyl-p-benzoquinone imine and 1, 4-benzoquinone [5]. Large quantities of ACT are discharged into water resources annually because of high consumption, low absorption in the body (ca. 5%−15%), and high solubility in the aquatic phase (12.78 g/L) [5, 6]. The presence of ACT, as an antipyretic pharmaceutical compound, is reported in the effluents and surface water resources [7]. Unfortunately, ACT is deficiently removed by conventional wastewater treatment processes such as sedimentation, adsorption, coagulation, and biological activated sludge process [4, 6]. Thus, the development of novel and dependable treatment processes for the degradation of such persistent compounds is highly needed. Advanced oxidation processes (AOPs) such as photocatalysis, sonocatalysis, catalytic ozonation, Fenton and Fenton-like processes are proposed as effective treatment methods for the degradation of recalcitrant organic contaminants owing to the generation of free oxidizing radicals especially hydroxyl radicals ($^{\bullet}OH$) as one of the most powerful oxidants [8-12]. In these treatment methods, the utilization of sulfate radicals ($SO_4^{\bullet-}$)-based advanced oxidation processes (SR-AOPs) has recently attracted growing attention because of their high effectiveness and affinity towards the decomposition of persistent organic contaminants [13-15]. In fact, $SO_4^{\bullet-}$ (2.5–3.1 V) has higher redox potential than that of $^{\bullet}OH$ (1.8–2.7 V) [16, 17]. Sulfate radicals generated from peroxymonosulfate (PMS) have exhibited a great potential to attack organic compounds through hydrogen and electron abstraction/addition similar to $^{\bullet}OH$ radicals [10]. To date, several heterogeneous metal oxide compounds (Fe_2O_3 [18], $CuFe_2O_4$ [19], Co_3O_4 [20] 3D-α-$Co(OH)_2$/nickel foam [21] etc.) are synthesized and utilized for the activation of PMS to generate $SO_4^{\bullet-}$ in the solution. Recently, carbonaceous activators in nano-size such as

carbon nanotubes (CNTs) [22], reduced graphene oxide [23] and activated carbon [24] are discovered as promising alternatives to metal oxide compounds in order to efficiently activate PMS for the formation of free radical species in the aquatic phase considering green remediation techniques. The metal-free nature of the nano-sized carbonaceous activators with the high specific surface area can play an excellent role as carbocatalyst in environmental remediation, hindering the leachate of toxic metals into various environments [10]. In most carbon-activated PMS processes, $SO_4^{\bullet-}$ and also $^{\bullet}OH$ are the main reactive oxidative species responsible for the degradation and removal of organic pollutants [25]. The formation of oxidizing radicals ($SO_4^{\bullet-}$ and $^{\bullet}OH$) in the graphene-activated PMS process is reported [26]. The contribution of the aforementioned radicals is also verified in the case of other carbonaceous compounds such as amorphous carbon spheres, activated carbon and mesoporous carbon [19, 22, 27]. Carbon-based compounds can donate e^- to PMS to generate reactive free radicals [28, 29]. Overall, both radical and nonradical decomposition mechanisms could occur on various carbon-based activators based on the structure of carbonaceous materials [10]. In the present study, as an innovative approach, carbon black nano-spheres (CBNS) were investigated for the activation of PMS to generate free radicals for the degradation of ACT drug in the liquid phase. As-prepared CBNS were immobilized into calcium alginate hydrogel matrix (CAHM) to avoid the washout of nanostructured activator from the reactor [30], improving reusability potential of the activator to be used in repeated runs of the full-scale operation. On the basis of our literature review, the application of CBNS for the activation of PMS, whether immobilized or not immobilized, is not investigated until now.

2. Materials and methods

2.1. Materials and devices

Sodium alginate extracted from *Laminaria hyperborean* was acquired from BDH Co. (England) for immobilization of the activator. The CBNS (Vulcan XC72R) used for the activation of PMS was prepared from Cabot Co. (USA). ACT ($C_8H_9NO_2$) as the target pollutant was purchased from Sigma-Aldrich (USA). All other chemicals including PMS were purchased from Merck Co. (Germany). For the immobilization, the CBNS was added to the viscous solution of sodium alginate (2 wt%) and then mechanically stirred until reaching homogeneity. The homogeneous mixture was dropwise added to the calcium chloride solution. As-formed CBNS/CAHM beads were withdrawn from the solution and dried in ambient air. Afterward, they were milled and stored in a desiccator until use. The procedure used for the synthesis of CBNS/CAHM is schematically illustrated in Fig. 1. Batch flow mode reactors were used for conducting the experiments. To evaluate the effect of UV light irradiation on the efficiency of the process, a 6-W low-pressure UVC lamp was used. An Elma ultrasonic bath (P30H, Germany) was implemented to assess the effect of ultrasound (US) on the reactor effectiveness.

2.2. Analyses and characterization

10-mL samples taken from batch flow mode experimental reactors were filtered and centrifuged for 5 min at 10000 rpm before the analysis. Ethanol (0.5 mL) was added to the sample to inhibit the oxidative activity of the residual PMS. High-performance liquid chromatography (HPLC) was implemented to measure the residual concentration of ACT in the solution after the treatment process of PMS/CBNS/CAHM. The instrument was equipped with a RP Amide column and a UV detector (absorbance wavelength: 243 nm). The mobile phase was a mixture of

methanol (60 vol.%) and deionized (DI) water (40 vol.%). The mobile phase flow-rate was set to 1 mL/min. Oxygen uptake rate (OUR) was determined using a portable dissolved oxygen meter (DO meter). Mineralization of the organic pollutant was checked using total organic carbon (TOC) analysis. Scanning electron microscopy (SEM) was applied to evaluate surface morphology of the samples (Tescan, Mira3, Czech Republic). Energy dispersive X-ray (EDX), along with elemental mapping, was performed to exhibit the elemental composition and distribution in the nanocomposite. X-ray diffraction (XRD) analysis (Philips, PW1730, Holland) was applied to visualize the structure of the activator (phase distribution) as well as its crystallinity. An Avatar Fourier transform infrared (FT-IR) spectrometer (Thermo Co, USA) was used to specify the functional groups placed on the surface of the activator samples. Magnetism of the samples containing electro-synthesized magnetite nanoparticles was examined via a vibrating sample magnetometer (VSM made by Kashan University).

2.3. Microbial community response

The microbial community response toward the ACT-contained solution after the treatment process was examined using microbial consortium. For this purpose, an activated sludge sample with mixed liquor volatile suspended solids (MLVSS) of about 2100 mg/L was obtained from a municipal wastewater treatment plant. The MLVSS was measured according to the procedure used in our previous work [31]. The OUR was measured after the addition of reactor effluent

containing ACT applying the portable oxygen probe. Finally, the inhibition percent was calculated based on the following equation:

$$\text{Inhibition percent (\%)} = \left[1 - \frac{\text{OUR}_S}{\text{OUR}_B}\right] \times 100 \qquad (1)$$

where OUR_B and OUR_S are the OUR values for the blank sample (without ACT) and the sample containing ACT, respectively.

2.4. Magnetic co-immobilization

In order to further enhance the reusability potential of the CBNS/CAHM carbocomposite, magnetite nanoparticles prepared through electrochemical process were used for magnetic co-immobilization of CBNS within CAHM. The procedure used for the preparation of magnetite nanoparticles is mentioned in our previous works [4, 32]. For the magnetic immobilization, electro-synthesized magnetite nanoparticles were removed from the electrochemical cell, dried and added to the viscous mixture of CBNS/CAHM. After homogenization, the mixture was added to calcium chloride solution. As-formed magnetic beads were separated and dried. Finally, they were milled and stored for conducting co-immobilization experiments.

3. Results and discussion

3.1. Characterization

SEM images of the obtained CBNS were taken at two different magnifications. Fig. 2 (a) and (b) show the uniform size distribution of CBNS with relatively regular shapes. As depicted in Fig. 2

(b), most of nano-spheres are in the size range of 5-15 nm with the frequency of 47%, indicating ultrafine size of the activator with abundant reaction sites for the efficient activation of PMS to produce more free radicals in the solution. Considering cumulative frequencies, about 78% of the nano-spheres are smaller than 30 nm which is remarkable. The immobilized form of nano-spheres is also shown in Fig. 2 (c) and (d). The images exhibit excellent entrapment of the nano-spheres within the hydrogel matrix. However, as can be seen, the nano-spheres and their active sites are available after the immobilization to effectively activate PMS molecules. The nano-spheres are well immobilized to avoid their washout from the reactor for utilization in repeated runs.

EDX micrographs of the pristine CBNS and CBNS/CAHM are also displayed in Fig. S1. Fig. S1 (a) shows the pure structure of as-prepared CBNS comprised of only carbon element. In the micrograph of the CBNS/CAHM composite, the peak related to calcium element is added to the micrograph with significant weight percent (wt%) of about 23% (Fig. S1 (b)). During the immobilization (see Fig. 1), calcium atoms of the calcium chloride solution cross link and create some salt bridges between the α-L-guluronic acids blocks present in the alginate chains. In fact, the presence of the calcium atom peak in the micrograph of CBNS/CAHM confirmed the proper entrapment of the activator nano-spheres.

Elemental mapping of the samples are shown in Fig. S2. The representative image of the CBNS and its corresponding mapping are exhibited in Fig. S2 (a) and (b). The uniform distribution of carbon element in the structure of as-obtained nano-spheres is apparent (Fig. S2 (b)). Fig. S2 (c) shows a representative image of the immobilized CBNS. In the case of the CBNS/CAHM composite, the elements (carbon and oxygen), along with the calcium atom, are well distributed,

confirming not only the presence of all elements in the nanocomposite but also their relatively uniform distribution in the composite (Fig. S2 (d-f)).

Surface functional groups play major role in the adsorption of target pollutant, immobilization process and the formation of free oxidizing radicals in the solution. For this, FT-IR spectra of both pure CBNS and CBNS/CAHM carbocomposite were recorded (Fig. 3). There are five main peaks in the spectrum of CBNS placed at around 3500, 2920, 1630, 1110 and 460 cm^{-1} which are attributed to the hydroxyl (O–H) groups [33], C–H stretching [34], vibration of absorbed water [7, 35], involvement of C–O–C groups [27], and C=O=C bonds [33], respectively. The presence of surface functional groups is beneficial to generate sulfate radical in the solution through the activation of PMS [19, 36]:

$$CBNS - OH + HSO_5^- \rightarrow CBNS + SO_4^{\bullet -} \quad (2)$$

$$CBNS - C = C = O + HSO_5^- \rightarrow CBNS - C = C - O^+ + SO_4^{\bullet -} + OH^+ \quad (3)$$

In fact, the moiety of OH groups on the surface of CBNS is known to play a positive role during the activation of PMS. In general, the oxygen functional groups placed on the defective edges of the activator are considered as the origin of the activation reaction. The intensity of the peaks placed at around 1630, 1110 and 460 cm^{-1} diminished after the immobilization, indicating the intensive entrapment of CBNS into the alginate matrix. Moreover, the peaks shifted to either lower wavenumber or higher wavenumber which implied the involvement of functional groups in the immobilization process. The weak peak located at 1702 cm^{-1} is associated with the C=O stretching of the COOH bond [37], which is advantageous for the improved dispersion of the carbocomposite in the solution as well as the binding [33]. Furthermore, as shown in Fig. 3 (b), the peaks at 1027 and 1068 cm^{-1} reveals the presence of guluronate and mannuronate of the

CAHM in the structure of carbocomposite [38]. The peak at 1631 cm^{-1} is also intensified after the incorporation of CBNS into the CAHM, which is ascribed to their abundance in the alginate matrix [37].

The patterns obtained during XRD analysis are displayed in Fig. S3. The pattern of CBNS exhibited the main peaks at 24.29 and 43.30° associated with the (002) and (100) planes of the carbo-compounds such as CBNS [4]. The peaks related to the carbonaceous compound of CBNS were diminished after its immobilization into alginate matrix. The pattern of CBNS immobilized within CAHM indicated non-crystalline (amorphous) structure of the obtained carbocomposite due to the existence of CAHM. The XRD pattern of the calcium alginate matrix does not exhibit sharp peaks [39]. The gelation process usually changes the spatial structure of alginate hydrogel, thus creating an amorphous structure even after the immobilization process. Actually, characteristic peaks of the CAHM are known to be appeared at 25.79, 31.19, 41.49, 49.04°, confirming the semi-crystalline nature of the carbocomposite containing alginate hydrogel. Calcium alginate is a linear polysaccharide comprised of both α-1,4-L-guluronic acid (G) and poly-β-1,4-D-mannuronic acid (M) with different ratios, which are organized in GG or MM blocks intermingled with MG blocks [37]. The main characteristic peak of alginate matrix, which is typically located at 2θ of 13.5° [39, 40], was not observed in the CBNS/CAHM carbocomposite pattern exhibiting the favorable incorporation of nano-spheres into the alginate lattice. This suggested the intermolecular interactions in the structure of as-synthesized carbocomposite and the overlapping of the CAHM and CBNS patterns in the combined XRD pattern [40].

3.2. Preliminary studies together with pH effect

The efficiency of CBNS/CAHM-activated PMS for the degradation of ACT was compared with other treatment options including PMS alone, PMS/CAHM and PMS/CBNS. The adsorption of ACT onto CAHM, CBNS and CBNS/CAHM carbocomposite was also assessed to evaluate its participation in finally measured removal efficiency of ACT. To determine the role of adsorption process, the following equation was applied:

$$Adsorption = \frac{(C_0 - C_e) \times V}{M} \qquad (4)$$

where C_0 and C_e are the initial and residual concentration of ACT (mg/L or mmole/L). The working volume and the activator dosage are represented through V (L) and M (g), respectively [41]. The linear form of the Langmuir isotherm equation was employed to determine the maximum adsorption capacity of the CAHM, CBNS and CBNS/CAHM carbocomposite to attain a valuable comparison as represented in the following equation [42, 43]:

$$\frac{C_e}{q_e} = \frac{1}{kq_m} + \frac{1}{q_m} C_e \qquad (5)$$

where q_m (q_{max}, mg/g or mmole/g) is the maximum adsorption capacity of the above-mentioned compounds, *K* is the affinity of adsorbent toward the adsorbates (L/mmole), and q_e (mg/g or mmole/g) is the adsorption capacity at equilibrium time. According to the results displayed in Fig. 4, the data are well-fitted to the Langmuir model with the maximum adsorption capacities of 2.5×10^{-2}, 3.5×10^{-2} and 3.1×10^{-2} mmole/g for the CAHM, CBNS and CBNS/CAHM carbocomposite, respectively. In conclusion, the adsorption process was not efficient to remove ACT molecules from the aquatic phase. The degradation of the target pollutant in the boundary layer placed on the external surface of the carbonaceous activator is confirmed and reported [24].

The analysis of data presented in Fig. 4 clearly indicated the insignificant efficiency of the sole use of PMS (28.1%) and PMS/CAHM (23.2%) to treat ACT solution with the initial concentration of 0.1 mM. The substantial efficiency of 65.4% was obtained when the treatment process of PMS/CBNS was implemented, suggesting the activating behavior of CBNS toward the PMS molecules to intensify the degradation of ACT. The intact sp^2-conjugated π structure in carbon-based activator and their electron-rich groups proposed as Lewis basic sites can activate the dissociation of HSO_5^- to generate both $SO_4^{\bullet-}$ and $^{\bullet}OH$ radicals, similar to what happens in the case of metal-based activation [10, 44]. The generation of sulfate radicals can be expressed by the following equation [36]:

$$CBNS - \pi^+ + HSO_5^- \rightarrow CBNS - \pi + OH^- + SO_4^{\bullet-} \quad (6)$$

The generation of sulfate radicals due to the electron transfer from the activator of powdered activated carbon (PAC) is observed and reported for the degradation of phenol by the catalyzed PMS [45]. The non-radical route of the degradation in the presence of carbon-based activators is also demonstrated. Both radical and non-radical mechanisms are proposed for the carbon-based activators to activate PMS [10, 44]. The defective edges at the border of carbonaceous matrix are capable to promote the degradation of refractory organics without the formation of radical species [10]. Functional groups placed on the defective edges can also play an important function in the catalytic reaction inducing a redox process [36]. The presence of several functional groups on the external surface of the immobilized CBNS is confirmed through the FT-IR analysis results. The PMS can be activated by the immobilized CBNS via three main routes: (1) radical path through the formation of $SO_4^{\bullet-}$ and $^{\bullet}OH$, (2) non-radical path through the creation of charge transfer complex, and (3) the integration of non-radical and radical paths. The schematic of the proposed paths for the transformation of ACT is illustrated in Fig. 5. As illustrated in Fig. 4, the

application of milled CBNS/CAHM as immobilized form of the activator resulted in the removal efficiency of 76.8%. This increase in the effectiveness may be attributed to the better dispersion of nano-spheres in the solution with lower aggregation due to the immobilization which creates more reactive sites for the interaction between the activator and PMS. Regardless of the increase in the degradation efficiency of ACT, the immobilization of nano-sized activator prevents the activator to be left from the reactor, thereby improving cost-effectiveness of the treatment process. This improves the chance of the treatment process for the full-scale implementation.

Operational conditions such as operating pH have a significant impact on the activation of PMS, further influencing the removal efficiency of the target organic pollutant. As shown in Fig. 4, at the end of the reaction time of 60 min, the degradation efficiencies (%) of ACT by the PMS/CBNS/CAHM process under acidic (pH: 3.0), natural (pH: 5.5), neutral (pH: 7.0) and basic (10.0) conditions were obtained 55.0, 76.8, 68.2, and 81.5%, respectively. Thus, basic pH is favored the degradation of ACT by the process. The existing form of PMS is remarkably influenced by the solution pH. Basic pH conditions favored the activation of PMS [13-15, 28]. In addition, hydrogen ions formed under strongly acidic conditions act as the scavenger for both $SO_4^{\bullet-}$ and $^{\bullet}OH$ radicals [28], leading to the diminished degradation of ACT under strongly acidic pH of 3.0. However, basic pH conditions caused insignificant enhancement in the degradation of ACT by the process compared with the natural pH conditions (lower than 10% increase). The reason for the obtained result is related to the pK_a value of ACT which is 9.5. Therefore, ACT molecule will be protonated as the initial solution pH exceeds 9.5, leading to the decreased reaction rate of the target pollutant degradation [8]. In addition, increasing the initial pH from natural to neutral value resulted in inconsiderable change in the degradation efficiency which may be attributed to the high reduction potential of $SO_4^{\bullet-}$ at neutral pH conditions, exhibiting

more selective decomposition of recalcitrant organic pollutants with aromatic structure and unsaturated bonds [46, 47]. Based on the Nernst equation, the oxidation potential of PMS decreases with increasing pH values which coincides with the reduction of hydrogen ions [H^+]:

$$E(HSO_5^- + HSO_4^-) = 1.85 + 0.0296\, lg[HSO_5^-][H^+]^2/[HSO_4^-](V\ vs.NHE) \quad (7)$$

Conclusively, the increased degradation of ACT at neutral pH conditions is due to the reaction of organic contaminants with the secondary byproducts of the activated PMS not direct reaction with PMS alone because of its weak oxidation potential at neutral pH. Considering the economic point of view and applicability, the following experiments were conducted under natural pH conditions without the need to pH adjustment.

3.4. Effects of amount of PMS, activator and target pollutant

The influence of three main operational parameters including PMS concentration, activator dosage and initial target pollutant (solute) concentration was assessed by varying ACT in the range of 0.05–0.3 mM, PMS in the range of 0.5–3.0 mM and CBNS/CAHM dosage in the range of 0.1 – 0.5 g/L, while the initial pH (natural pH of 5.5) and the reaction time (60 min) was kept constant during the experiments. Accordingly, increasing both PMS concentration and the activator dosage led to the enhanced degradation of ACT (Fig. 6). In the presence of the activator dosage of 0.3 g/L, the degradation efficiency of ACT increased from 38.4 to 91.4% when the concentration of PMS increased from 0.5 to 3.0 mM, respectively. The dependence of the degradation of target pollutant on the concentration of PMS is in accordance with the investigations implementing transition metals-activated PMS [16]. At the constant PMS concentration of 1 mM, the degradation efficiency increased from 56.3 to 78.8% as the dosage of

activator increased in the range of 0.1 – 0.5 g/L. Utilization of higher amounts of carbocomposite provides more reactive sites for the activation of PMS, generating more radical species for the degradation of ACT. At the maximum PMS concentration of 3 mM, rise in the degradation efficiency of ACT was negligible when the dosage of activator increased from 0.1 to 0.3 g/L, which indicated the importance of the determination of the optimum value of the activator for the treatment process. It is noteworthy that an excessive increase in the amount of carbocomposite particles leads to their aggregation in the bulk solution, hindering the efficient activation of PMS. In fact, the available reactive sites for the activation of PMS are reduced as a result of excessive use of carbocomposite. In the case of the effect of ACT concentration on its degradation efficiency, more than 70% reduction in the efficiency occurred as the initial solute concentration increased in the range of 0.05-0.3 mM. The complete degradation of ACT (100%) happened at the initial concentration of 0.05 mM. Obviously, increasing the concentration of solute diminished the effectiveness of the treatment process due to the fact that higher amounts of oxidizing agents are required to decompose higher concentrations of the target pollutant.

3.5. Influence of nutrients

The discharge of nutrients including nitrogenous and phosphorous compounds into the environment is one of the major environmental concerns. Hence, the presence of such compounds in the water resources and subsequently industrial and municipal wastewaters is unavoidable. Accordingly, determination of the impact of these compounds on the efficiency of the treatment process of PMS/CBNS/CAHM can be useful to assess the process performance under real conditions. Based on the presented results, the degradation of ACT was not remarkably affected by the presence of nitrate, nitrite and ammonium ions as the most abundant nitrogenous compounds. In the presence of nitrate, nitrite and ammonium ions, the degradation

efficiencies (%) of ACE decreased from 76.8 to 71.2, 65.4 and 70.5%, respectively (Fig. 7 (a)). Similar trends were observed and reported for the decomposition of organic pollutants by the PMS-based treatment processes when nitrate ions were added to the reactor [48, 49]. The presence of phosphate anion enhanced the degradation of ACT by the PMS-based treatment process (81.9%). It is demonstrated that the application of phosphate buffer solution leads to the enhanced activation of PMS to generate more $SO_4^{\bullet-}$ in the solution [16].

3.6. Effect of hardness and alkalinity

Hardness and alkalinity are two major characteristics of water resources. In the case of alkalinity, main anions-causing alkalinity (both bicarbonate and carbonate ions) are present in natural water resources and consequently wastewater in high concentrations [50]. Due to the geology of groundwater (underground aquifers) with high calcite and dolomite content, this type of water resource has a high concentration of calcium and magnesium ions causing hardness in the natural groundwater water. For this, the effect of these two indicators and their compartments on the carboactivation of PMS was evaluated to attain the potential of the treatment process for the water decontamination (Fig. 7 (b)). Based on the data presented in Fig. 7 (b), the hardness of water slightly reduced the degradation efficiency of ACT by the PMS/CBNS/CAHM process. Similar results are reported by Park et al., in their study on the degradation of trichloroethylene (TCE) by the activated PMS [51]. Generally, hardness-causing ions including calcium and magnesium cations can deactivate the activator and blocks its active reaction sites, resulting in the diminished generation of free radical species in the reactor [52]. As displayed in Fig. 7 (b), among cations causing hardness, the magnesium ions decreased the degradation efficiency of

ACT by about 10%. The effect of carbonaceous system (carbonate and bicarbonate ions) causing alkalinity in the bulk solution was also studied. The alkalinity of the water body is an important parameter which results in the stability of water in related facilities owing to improving its buffering capacity [53]. Thus, the evaluation of the effect of this parameter and its components on the process performance is reasonable. Fig. 7 (b) exhibited that the alkalinity of water diminishes the degradation efficiency of ACT. Based on the Nernst equation (see Eq. 7), the oxidation potential of PMS decreases with increasing pH (reduction of hydrogen ions) due to the presence of alkalinity causing anions [16]. Sulfate radicals react with bicarbonate and carbonate anions generating bicarbonate and carbonate radicals which can serve as oxidizing agents to decompose ACT drug. Nevertheless, the oxidizing potential of both bicarbonate and carbonate is lower than sulfate radicals [53, 54]:

$$SO_4^{\bullet-} + HCO_3^- \rightarrow HCO_3^{\bullet} + SO_4^{2-} \quad (8)$$

$$SO_4^{\bullet-} + CO_3^{2-} \rightarrow CO_3^{\bullet} + SO_4^{2-} \quad (9)$$

$$HCO_3^{\bullet} \rightarrow CO_3^{\bullet-} + H^+ \quad (10)$$

The negative effect of carbonate and bicarbonate ions on the activation of PMS and quenching sulfate and hydroxyl radicals is observed and reported [28]. According to Fig. 7 (b), the presence of bicarbonate anion led to a further reduction in the degradation efficiency in comparison with carbonate ions. Guan et al. reported that the initial concentration of bicarbonate anions is important concerning the inhibitive effect of bicarbonate on the degradation of atrazine by the activated PMS [55]. Unlike the hardness, the alkalinity of water with equal amounts of both bicarbonate and carbonate anions led to the further decrease of degradation efficiency compared with the individual anions. Overall, based on the obtained data, PMS-mediated oxidation of ACT

catalyzed by the CBNS/CAHM may not be significantly influenced in real water samples such as groundwater containing inorganic cations and anions.

3.7. Scavenging study

The present study only evaluated the performance of carbon-based material of CBNS/CAHM for the activation of PMS in order to degrade one pollutant. Due to the presence of several organic pollutants in the real wastewater, further investigations are required to examine the effectiveness of CBNS/CAHM to activate PMS when various organic pollutants exist in the liquid stream simultaneously. Moreover, the negative effect of the presence of some co-exiting compounds on the degradation efficiency of the target pollutant indicates the role of free oxidizing species in the degradation of target organic contaminant. For the latter purpose, ethanol, para-benzoquinone (PBQ), *tert*-butanol, methanol, humic acid, formic acid, ethylenediaminetetraacetic acid (EDTA), and glucose were added to the reactor and the efficiency of the reactor was determined in the presence of aforementioned compounds (Fig. 7 (c)). The reaction rate constant of t-butanol with $^{\bullet}OH$ is in the range of 3.8–7.6×10^8 M^{-1} s^{-1}, approximately 418–1900 times higher than that of the $SO_4^{\bullet-}$ (4.0–9.1×10^5 M^{-1} s^{-1}). Therefore, t-butanol is often an $^{\bullet}OH$ scavenger rather than a $SO_4^{\bullet-}$ scavenger [24, 48]. Based on the obtained results, the addition of 0.01 M t-butanol did not significantly suppress the degradation efficiency of ACT, indicating that $^{\bullet}OH$ is not the main radical form responsible for the decomposition. A similar result was obtained when 0.01 M methanol recognized as both $^{\bullet}OH$ (9.7×10^8 M^{-1} s^{-1}) and $SO_4^{\bullet-}$ scavenger (2.5×10^7 M^{-1} s^{-1}) was added to the reactor [54]:

$$SO_4^{\bullet-} + MeOH \rightarrow {}^{\bullet}CH_2OH + SO_4^{2-} + H^+ \qquad k = 2.5 \times 10^7\ M^{-1}\ s^{-1} \qquad (11)$$

$$^{\bullet}OH + MeOH \rightarrow {}^{\bullet}CH_2OH + H_2O \qquad k = 9.7 \times 10^8\ M^{-1}\ s^{-1} \qquad (12)$$

Ethanol, as both $^{\bullet}OH$ ($1.2–2.8 \times 10^9\ M^{-1}\ s^{-1}$) and $SO_4^{\bullet-}$ scavenger ($1.6–7.7 \times 10^9\ M^{-1}\ s^{-1}$) in the similar rate [56], caused the most suppressive effect on the degradation efficiency of the treatment process of PMS/CBNS/CAHM. In the presence of ethanol, the degradation efficiency decreased from 76.8 to 51.4%. Therefore, the results demonstrated the involvement of both $SO_4^{\bullet-}$ and $^{\bullet}OH$ radicals in the degradation of ACT and domination of $SO_4^{\bullet-}$ radicals in the degradation process. Formic acid caused an insignificant effect on the degradation of ACT by the PMS/CBNS/CAHM process. Although it is reported that the addition of EDTA can improve the activity of iron ions for the activation of PMS [57], this compound did not significantly influence the effectiveness of the PMS/CBNS/CAHM process. This may be related to the different nature of the activator used in the present investigation which is a nonmetal activator. The structure of humic substances is complicated as they are high molecular weight compounds. Based on the results, humic acid brought about an insignificant decrease in the removal efficiency of ACT. The humic substances such as humic acid scavenge positive holes placed on the catalyst surface at low pH and scavenge radicals at high pH. Thus, the quenching of the as-generated radicals by the humic acid at natural pH value of 5.5 and consequently decreasing the degradation efficiency is not expected in the present study. Furthermore, quinones and hydroquinones compounds in the structure of humic acid macromolecule can play as activator of the PMS preventing its scavenging properties [50]. This fact can be confirmed by the results obtained in the presence of parabenzoquinone (PBQ). As shown, the presence of PBQ not only did not reduce the degradation efficiency of ACT but also insignificantly increased the efficiency. It is noteworthy that the PBQ is recognized as superoxide anion radical ($O_2^{\bullet-}$) scavenger; thus, this type of radical species was not involved in the degradation of ACT [58]. Overall, it has been demonstrated that

the presence of carbon-based activators abates the detrimental impact of radical scavenging compounds on the process performance [59]. This is one of the reasons why co-existing compounds do not remarkably affect the degradation efficiency of the treatment process. In the worst cases, <30% reduction in the degradation efficiency was observed. From another point of view, not much reduction in the degradation efficiency of ACT in the presence of free radical scavenging compounds indicated an irreplaceable role of non-radical mechanisms in the decomposition of ACT. These findings are hopeful for the application of such treatment process to treat real wastewaters containing many organic and inorganic species.

3.8. Process enhancement options

To further improve the effectiveness of the treatment process, enhancing the potential of some physical and chemical agents including ultraviolet (UV) radiation, ultrasound (US) irradiation, persulfate (PS) and percarbonate (PC) was appraised. Fig. 7 (d) displays the positive effect of both UV and US on the effectiveness of the reactor [32, 56]:

$$SO_5^- \xrightarrow{UV\ or\ US} SO_4^{\bullet-} + {}^{\bullet}OH \qquad (13)$$

The efficiency increased from 76.8 to 93.3 and 89.0% when the reactor was assisted with UV and US radiation, respectively. The PMS will be activated by the UV radiation, leading to the cleavage of peroxide bond, which simultaneously provides sulfate and hydroxyl radicals for the decomposition of ACT [50]. In addition, US irradiation converts the sulfate radicals into hydroxyl radicals with substantial oxidation activity [60]:

$$SO_4^{\bullet-} + H_2O \xrightarrow{US} SO_4^{2-} + {}^{\bullet}OH + H^+ \qquad (14)$$

Sonocavitation, caused by US, is a physical process including the rapid generation, growth and intense collapse of cavitation bubbles in the liquid phase, which results in the production of •OH. As-generated radicals non-selectively react with the pollutant present in the water [61]. As an enhancer, the presence of PS not only did not amplify the decomposition of ACT, but also reduced the decomposition efficiency from 76.8 to 69.7%, attributing to the side reaction between PS ions and sulfate radicals as the main oxidizing species of the PMS/CBNS/CAHM process [62]:

$$S_2O_8^{2-} + SO_4^{\bullet-} \rightarrow S_2O_8^{\bullet-} + SO_4^{2-} \quad (15)$$

The addition of PC also diminished the decomposition efficiency of ACT. This may be as a result of scavenging properties of the hydrogen peroxide content of the PC at specific concentration, creating hydroperoxyl radical (HOO•) instead of hydroxyl radical with lower oxidation potential as displayed below [32, 63]:

$$2Na_2CO_3 \cdot 3H_2O_2 \rightarrow 2Na_2CO_3 + 3H_2O_2 \quad (16)$$

$$H_2O_2 + HO^{\bullet} \rightarrow HOO^{\bullet} + H_2O \quad (17)$$

It is notable that the transformation of •OH to HOO• diminishes the oxidizing capacity of the treatment system.

3.9. Stability and magnetization

As-prepared CBNS were immobilized within CAHM to avoid their release into the effluent. It seems that it is advantageous to increase the capability of the carbocomposite to be used within multiple operational runs without significant loss in the carboactivation capacity. Nevertheless,

since the carbonaceous compounds may lose their capacity after repeated experimental runs as a result of the surface deactivation; thus, it is essential to evaluate the stability of the CBNS/CAHM carbocomposite within consecutive runs. In this regard, the carbocomposite was used within five repeated runs and the degradation efficiency of ACT was recorded after each run. The data presented in Fig. 8 (a) showed the negligible drop in the degradation efficiency of ACT after five experimental runs. At the end of the fifth run, the reduction was lower than 10%. This result indicated the high stability of immobilized CBNS improved with the aid of CAHM. Actually, the separation of ultrafine particles of non-immobilized CBNS from the reactor was not feasible at all. The insignificant reduction in the efficiency after fifth cycle may be related to the minor loss of activator particles during the separation and drying process before the next run.

In the next step, as-prepared CBNS were co-immobilized with magnetite (Fe_3O_4) nanoparticles. Furthermore, magnetite (Fe_3O_4) with stable physiochemical structure, easy and low-cost preparation process and sensitive magnetic response is proposed as a promising activator of the PMS. Interestingly, this approach improved the reusability potential of the carbocomposite as well as its carboactivation ability to enhance the formation of sulfate radicals in the PMS-based treatment reactor. The degradation efficiency increased to 95.6% owing to the incorporation of magnetite nanoparticles into the CBNS/CAHM carbocomposite (Fig. 8 (b)). The inverse spinel cubic structure of magnetite (Fe_3O_4) activates the O–O bond of the PMS to form more sulfate radicals in the solution [56]. Fig. 8 (c) demonstrated the formation of magnetite (XRD pattern) during the electrochemical synthesis. The main peaks located at 30.54, 35.89, 43.44, 53.79, 57.49, 62.94 and 74.39^o correspond to the (220), (311), (400), (422), (511), (440) and (533) planes of the structure of magnetite, respectively (JCPDS card no. 19–0629). The SEM image also confirmed the production of nanostructured magnetite due to the corrosion of anode during

the electrochemical process. Fig. 8 (d) showed the appropriate magnetic properties of the magnetite nanoparticles even after the entrapment within polymeric matrix of the alginate. The regeneration of the transition metals such as iron ions through the generation of sulfate radicals is expected, intensifying the activation process. The production of $^{\bullet}OH$ is also predictable due to the interaction of as-generated sulfate radicals with water molecules [64]. Due to implementing entrapped magnetite nanostructures, the above reactions intensified the reactor performance altogether.

3.10. Mineralization and microbial community response

The TOC removal of ACT was not more than 18.0% after the reaction time of 60 min, indicating that the target pharmaceutical pollutant can be partially mineralized during the PMS/CBNS/CAHM process. Lou and coworkers reported a similar result regarding the degradation of Acid Orange 7, Rhodamine B and 2,4,6-trichlorophenol by the activated PMS [16]. The PMS/CBNS/CAHM process results in the break-up and degradation of the parent pharmaceutical compound into small byproduct molecules, which may be difficult to be further destroyed and mineralized to inorganic species by the treatment process [24]. In addition, the coverage of the activator surface by the as-generated intermediate byproducts induces the deactivation of CBNS resulting in reduced mineralization [45]. The release of CBNS with nano-size into the bulk solution even after the immobilization was a great concern in the present study because the released carbon particles lead to worsening the quality of the reactor effluent. However, during a confirmatory experimental run, the results of TOC analysis showed no change in the organic content of the solution when the immobilized CBNS were added to the

ACT-contained reactor and agitated within the reaction time of 60 min. Therefore, the immobilization of fine carbon black spheres prevented their release into the bulk solution. The effluent of the PMS/CBNS/CAHM process was fed to the activated sludge containing microbial consortium to show the inhibitory effect of the effluent on living organisms of the ecosystem. According to the data provided in Table 1, the calculated inhibition percent increased from 29.08 to 47.52% when the effluent of the process was added after the reaction time of 10 min. It may be associated with the generation of toxic intermediate byproducts in the early minutes of the process. At the end of the reaction time of 60 min, the inhibition percent decreased to 9.93%, confirming the generation of effluent with lower toxicity than that of untreated ACT-contained solution. Although the mineralization efficiency of the sulfate radical-based process was insufficient, the operation of the process is probably led to the formation of organic intermediates with lower toxicity than the parent compound. Higher reaction time is required to achieve complete mineralization.

4. Conclusions

The CBNS were successfully applied for the activation of PMS to generate free oxidizing radicals especially sulfate radicals in the ACT-polluted water. To prevent the release of ultrafine particles of the CBNS into the environment, CAHM was applied as immobilizing agent for the entrapment of the nanostructured activator. The results indicated efficient immobilization of the CBNS with high activating potential even after the entrapment within the polymeric matrix. Surface functional groups analysis exhibited the involvement of oxygen-contained groups in the

activation of PMS and the subsequent generation of free radicals. The efficiency of the PMS/CBNS/CAHM process was dependent on the activator dosage, solute concentration and PMS dosage. The process was efficient for degrading low concentrations of ACT. The presence of other ionic species (calcium, magnesium, carbonate and bicarbonate ions) did not significantly affect the process efficiency. Interestingly, the presence of phosphate ions enhanced reactor performance. The scavenging compound of ethanol caused the highest suppressive effect on the formation of radical species in the solution, which implied the main role of sulfate radicals in the degradation of ACT molecules because t-butanol led to lower adverse effect than that of ethanol. The influence of natural organic matters was in overall not significant on the performance of the developed treatment process. The high reusability potential of the carbocomposite of CBNS/CAHM was observed. Magnetite nanoparticles incorporated into the carbocomposite not only improved the reusability of the activator particles but also enhanced the degradation of ACT owing to the intensified activation of PMS. Conclusively, the treatment process of PMS/CBNS/CAHM was an effective technique for the decontamination of pharmaceuticals-polluted water streams with high capability to be applied in full scale of the operation and low toxicity against living organisms.

Declaration of interests

The authors declare that they have no known competing financial interests or personal relationships that could have appeared to influence the work reported in this paper.

Acknowledgments

The support of Arak University of Medical Sciences is greatly appreciated. Prof. Grzegorz Boczkaj acknowledges the financial support from National Science Center, Warsaw, Poland – decision no. UMO-2017/25/B/ST8/01364.

References

[1] R.D.C. Soltani, M. Mashayekhi, M. Naderi, G. Boczkaj, S. Jorfi, M. Safari, Ultrasonics Sonochemistry, 55 (2019) 117-124.

[2] R. Darvishi Cheshmeh Soltani, M. Mashayekhi, Chemosphere, 194 (2018) 471-480.

[3] E. Szabados, G. Sági, F. Somodi, B. Maróti, D. Srankó, A. Tungler, Journal of Industrial and Engineering Chemistry, 46 (2017) 364-372.

[4] R. Mirzaee, R. Darvishi Cheshmeh Soltani, A. Khataee, G. Boczkaj, Journal of Molecular Liquids, 284 (2019) 536-546.

[5] Y. Li, Y. Pan, L. Lian, S. Yan, W. Song, X. Yang, Water Research, 109 (2017) 266-273.

[6] S. Wang, J. Wu, X. Lu, W. Xu, Q. Gong, J. Ding, B. Dan, P. Xie, Chemical Engineering Journal, 358 (2019) 1091-1100.

[7] C. Tan, N. Gao, Y. Deng, J. Deng, S. Zhou, J. Li, X. Xin, Journal of Hazardous Materials, 276 (2014) 452-460.

[8] Y. Zhang, Q. Zhang, J. Hong, Applied Surface Science, 422 (2017) 443-451.

[9] J. Fan, H. Qin, S. Jiang, Chemical Engineering Journal, 359 (2019) 723-732.

[10] X. Duan, Z. Ao, L. Zhou, H. Sun, G. Wang, S. Wang, Applied Catalysis B: Environmental, 188 (2016) 98-105.

[11] M. Gągol, A. Przyjazny, G. Boczkaj, Chemical Engineering Journal, 338 (2018) 599-627.

[12] R. Darvishi Cheshmeh Soltani, A.R. Khataee, M. Mashayekhi, Desalination and Water Treatment, 57 (2016) 13494-13504.

[13] R.D.C. Soltani, M. Mashayekhi, S. Jorfi, A. Khataee, M.-J. Ghanadzadeh, M. Sillanpää, Chemosphere, 210 (2018) 699-708.

[14] A. Fernandes, P. Makoś, G. Boczkaj, Journal of Cleaner Production, 195 (2018) 374-384.

[15] A. Fernandes, P. Makoś, J.A. Khan, G. Boczkaj, Journal of Cleaner Production, 208 (2019) 54-64.

[16] X. Lou, L. Wu, Y. Guo, C. Chen, Z. Wang, D. Xiao, C. Fang, J. Liu, J. Zhao, S. Lu, Chemosphere, 117 (2014) 582-585.

[17] G.P. Anipsitakis, D.D. Dionysiou, Environmental Science & Technology, 38 (2004) 3705-3712.

[18] N. Jaafarzadeh, F. Ghanbari, M. Ahmadi, Chemosphere, 169 (2017) 568-576.

[19] W.-D. Oh, S.-K. Lua, Z. Dong, T.-T. Lim, Journal of Hazardous Materials, 284 (2015) 1-9.

[20] P. Hu, M. Long, Applied Catalysis B: Environmental, 181 (2016) 103-117.

[21] R. Yuan, M. Jiang, S. Gao, Z. Wang, H. Wang, G. Boczkaj, Z. Liu, J. Ma, Z. Li, Chemical Engineering Journal, 380 (2020) 122447.

[22] C. Guan, J. Jiang, C. Luo, S. Pang, Y. Yang, Z. Wang, J. Ma, J. Yu, X. Zhao, Chemical Engineering Journal, 337 (2018) 40-50.

[23] H. Sun, S. Liu, G. Zhou, H.M. Ang, M.O. Tadé, S. Wang, ACS Applied Materials & Interfaces, 4 (2012) 5466-5471.

[24] J. Zhang, X. Shao, C. Shi, S. Yang, Chemical Engineering Journal, 232 (2013) 259-265.

[25] H. Sun, X. Peng, S. Zhang, S. Liu, Y. Xiong, S. Tian, J. Fang, Bioresource Technology, 241 (2017) 244-251.

[26] X. Duan, Z. Ao, H. Sun, S. Indrawirawan, Y. Wang, J. Kang, F. Liang, Z.H. Zhu, S. Wang, ACS Applied Materials & Interfaces, 7 (2015) 4169-4178.

[27] S. Yang, T. Xiao, J. Zhang, Y. Chen, L. Li, Separation and Purification Technology, 143 (2015) 19-26.

[28] J. Wang, S. Wang, Chemical Engineering Journal, 334 (2018) 1502-1517.

[29] M. Alikarami, R. Darvishi Cheshmeh Soltani, A. Khataee, Separation and Purification Technology, 220 (2019) 42-51.

[30] S. Zeng, X. Jin, D. Rajarathnam, Z. Chen, Journal of Industrial and Engineering Chemistry, 77 (2019) 238-242.

[31] R. Darvishi Cheshmeh Soltani, A. Rezaee, A.R. Khataee, H. Godini, The Canadian Journal of Chemical Engineering, 92 (2014) 13-22.

[32] F. Sepyani, R. Darvishi Cheshmeh Soltani, S. Jorfi, H. Godini, M. Safari, Journal of Environmental Management, 224 (2018) 315-326.

[33] H. Liu, W.-R. Cao, Y. Su, Z. Chen, Y. Wang, Journal of Colloid and Interface Science, 398 (2013) 161-167.

[34] F. Ali, S.B. Khan, T. Kamal, Y. Anwar, K.A. Alamry, A.M. Asiri, Chemosphere, 188 (2017) 588-598.

[35] M.E. Rincón, M.E. Trujillo-Camacho, A.K. Cuentas-Gallegos, N. Casillas, Applied Catalysis B: Environmental, 69 (2006) 65-74.

[36] R. Xiao, Z. Luo, Z. Wei, S. Luo, R. Spinney, W. Yang, D.D. Dionysiou, Current Opinion in Chemical Engineering, 19 (2018) 51-58.

[37] C. Larosa, M. Salerno, J.S. de Lima, R. Merijs Meri, M.F. da Silva, L.B. de Carvalho, A. Converti, International Journal of Biological Macromolecules, 115 (2018) 900-906.

[38] K. Sakugawa, A. Ikeda, A. Takemura, H. Ono, Journal of Applied Polymer Science, 93 (2004) 1372-1377.

[39] R. Zhang, L. Lei, Q. Song, X. Li, Colloids and Surfaces B: Biointerfaces, 175 (2019) 569-575.

[40] J. Li, J. Ma, S. Chen, J. He, Y. Huang, Food Hydrocolloids, 82 (2018) 363-369.

[41] M. Safari, A. Khataee, R.D.C. Soltani, R. Rezaee, Journal of Colloid and Interface Science, 522 (2018) 228-241.

[42] R. Darvishi Cheshmeh Soltani, A. Rezaee, G. Shams Khorramabadi, K. Yaghmaeian, Water Science and Technology, 63 (2011) 129-135.

[43] R.D.C. Soltani, A.J. Jafari, G.S. Khorramabadi, American Journal of Environmental Sciences, 5 (2009) 41.

[44] J. Chen, L. Zhang, T. Huang, W. Li, Y. Wang, Z. Wang, Journal of Hazardous Materials, 320 (2016) 571-580.

[45] E. Saputra, S. Muhammad, H. Sun, S. Wang, RSC Advances, 3 (2013) 21905-21910.

[46] Y.-H. Guan, J. Ma, X.-C. Li, J.-Y. Fang, L.-W. Chen, Environmental Science & Technology, 45 (2011) 9308-9314.

[47] M.G. Antoniou, A. Armah, D.D. Dionysiou, Applied Catalysis B: Environmental, 96 (2010) 290-298.

[48] C. Qi, X. Liu, J. Ma, C. Lin, X. Li, H. Zhang, Chemosphere, 151 (2016) 280-288.

[49] Y. Fan, Y. Ji, D. Kong, J. Lu, Q. Zhou, Journal of Hazardous Materials, 300 (2015) 39-47.

[50] S. Verma, S. Nakamura, M. Sillanpää, Chemical Engineering Journal, 284 (2016) 122-129.

[51] K.-M. Park, H.-K. Lee, S.-H. Do, S.-H. Kong, Degradation of TCE using persulfate (PS) and peroxymonosulfate (PMS): Effect of inorganic ions in groundwater, pp. 20-22, (2010).

[52] A.R.L. Ribeiro, N.F. Moreira, G.L. Puma, A.M. Silva, Chemical Engineering Journal, 363 (2019) 155-173.

[53] L. Hu, G. Zhang, M. Liu, Q. Wang, P. Wang, Chemical Engineering Journal, 338 (2018) 300-310.

[54] M. Jiang, J. Lu, Y. Ji, D. Kong, Water Research, 116 (2017) 324-331.

[55] Y.-H. Guan, J. Ma, Y.-M. Ren, Y.-L. Liu, J.-Y. Xiao, L.-q. Lin, C. Zhang, Water Research, 47 (2013) 5431-5438.

[56] J. Liu, J. Zhou, Z. Ding, Z. Zhao, X. Xu, Z. Fang, Ultrasonics Sonochemistry, 34 (2017) 953-959.

[57] J. Wang, M. Yang, R. Liu, C. Hu, H. Liu, J. Qu, Water Research, 160 (2019) 454-465.

[58] Y. Long, S. Bu, Y. Huang, Y. Shao, L. Xiao, X. Shi, Chemosphere, 216 (2019) 545-555.

[59] P.-S. Yap, T.-T. Lim, Applied Catalysis B: Environmental, 101 (2011) 709-717.

[60] M.P. Rayaroth, U.K. Aravind, C.T. Aravindakumar, Environmental Chemistry Letters, 14 (2016) 259-290.

[61] M. Gągol, R.D.C. Soltani, A. Przyjazny, G. Boczkaj, Ultrasonics Sonochemistry, 58 (2019) 104610.

[62] A. Ledjeri, I. Yahiaoui, F. Aissani-Benissad, Journal of Environmental Management, 184 (2016) 249-254.

[63] S. Sajjadi, A. Khataee, R. Darvishi Cheshmeh Soltani, N. Bagheri, A. Karimi, A. Ebadi Fard Azar, Journal of Industrial and Engineering Chemistry, 68 (2018) 406-415.

[64] G. Nie, J. Huang, Y. Hu, Y. Ding, X. Han, H. Tang, Chinese Journal of Catalysis, 38 (2017) 227-239.

Fig. 1. Schematic of the procedure used for synthesis of the activator.

Fig. 2. SEM images of CBNS (a and b) and its immobilized form (c and d).

Fig. 3. FT-IR spectra of CBNS and CBNS/CAHM.

Fig. 4. Contribution of each process to the removal of ACT (Experimental conditions: $[ACT]_0$ = 0.1 mM, $[PMS]_0$ = 1 mM, carbocomposite dosage = 0.3 g/L, pH = natural (5.5)), together with the influence of initial pH (pH values = acidic (3.0), natural (5.5), neutral (7.0), basic (10.0)) on effectiveness of the PMS/CBNS/CAHM process.

Fig. 5. Proposed paths responsible for the transformation of ACT by using PMS/CBNS/CAHM process.

Fig. 6. Variations in the degradation efficiency of ACT by the PMS/CBNS/CAHM process as the function of PMS concentration, activator dosage and initial solute concentration. Experimental conditions: $[ACT]_0$ = 0.05–0.3 mM, $[PMS]_0$ = 0.5–3.0 mM, carbocomposite dosage = 0.1 – 0.5 g/L, pH = natural (5.5), reaction time = 60 min.

Fig. 7. Effect of water matrix including nutrients (a), hardness and alkalinity (b), organic scavengers (c), and enhancers (d) on the reactor performance. Experimental conditions: $[ACT]_0$ = 0.1 mM, $[PMS]_0$ = 1 mM, carbocomposite dosage = 0.3 g/L, pH = natural (5.5), reaction time = 60 min, $[\text{co-existing compounds}]_0$ = 0.01 M.

Fig. 8. Results of reusability test (a), co-immobilization efficiency (b), SEM image and XRD pattern of the magnetite nanoparticles (c) and magnetic characterization of the magnetite sample before and after the immobilization (smaller graph) (d). Experimental conditions: $[ACT]_0$ = 0.1

mM, $[PMS]_0$ = 1 mM, carbocomposite dosage = 0.3 g/L, pH = natural (5.5), reaction time = 60 min.

Fig. 1

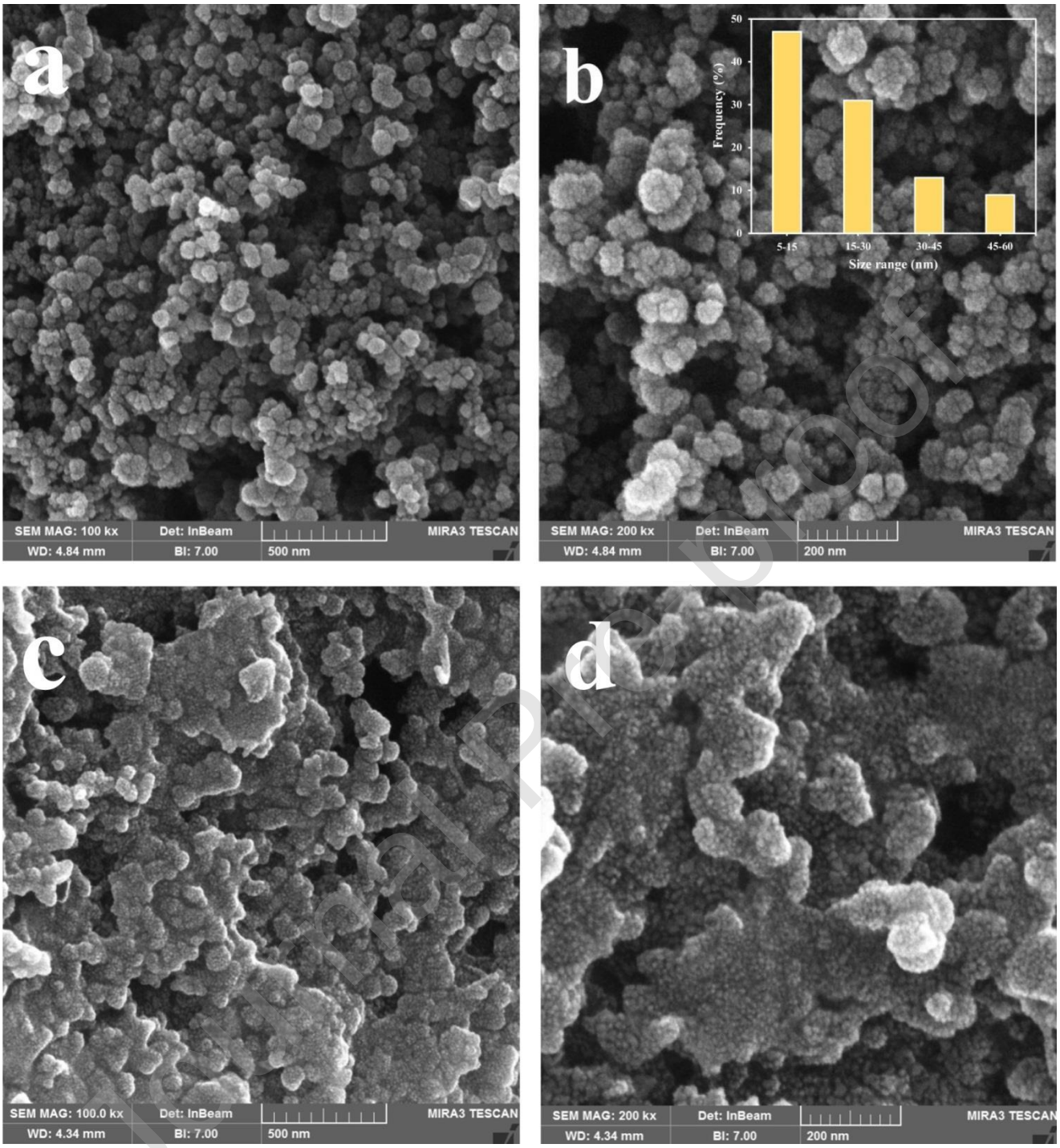

Fig. 2

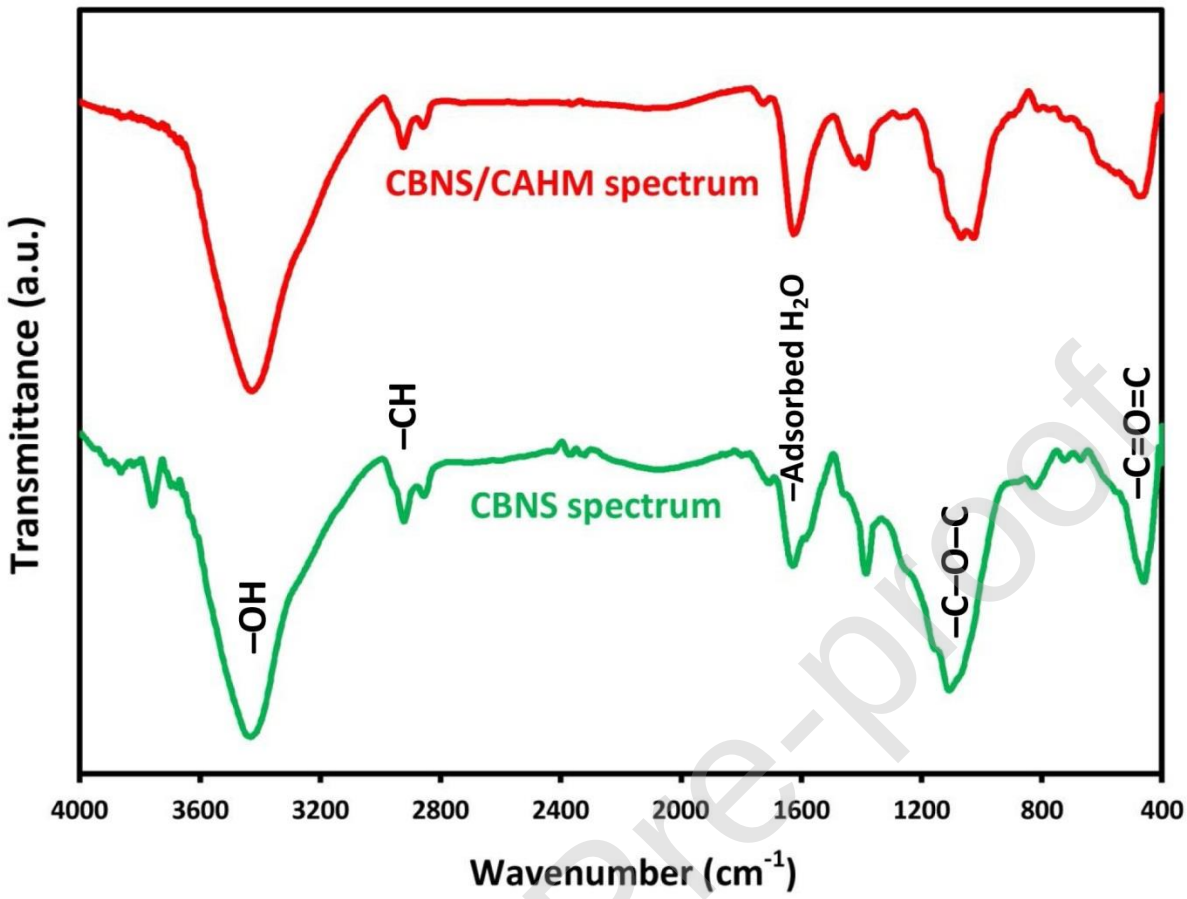

Fig. 3

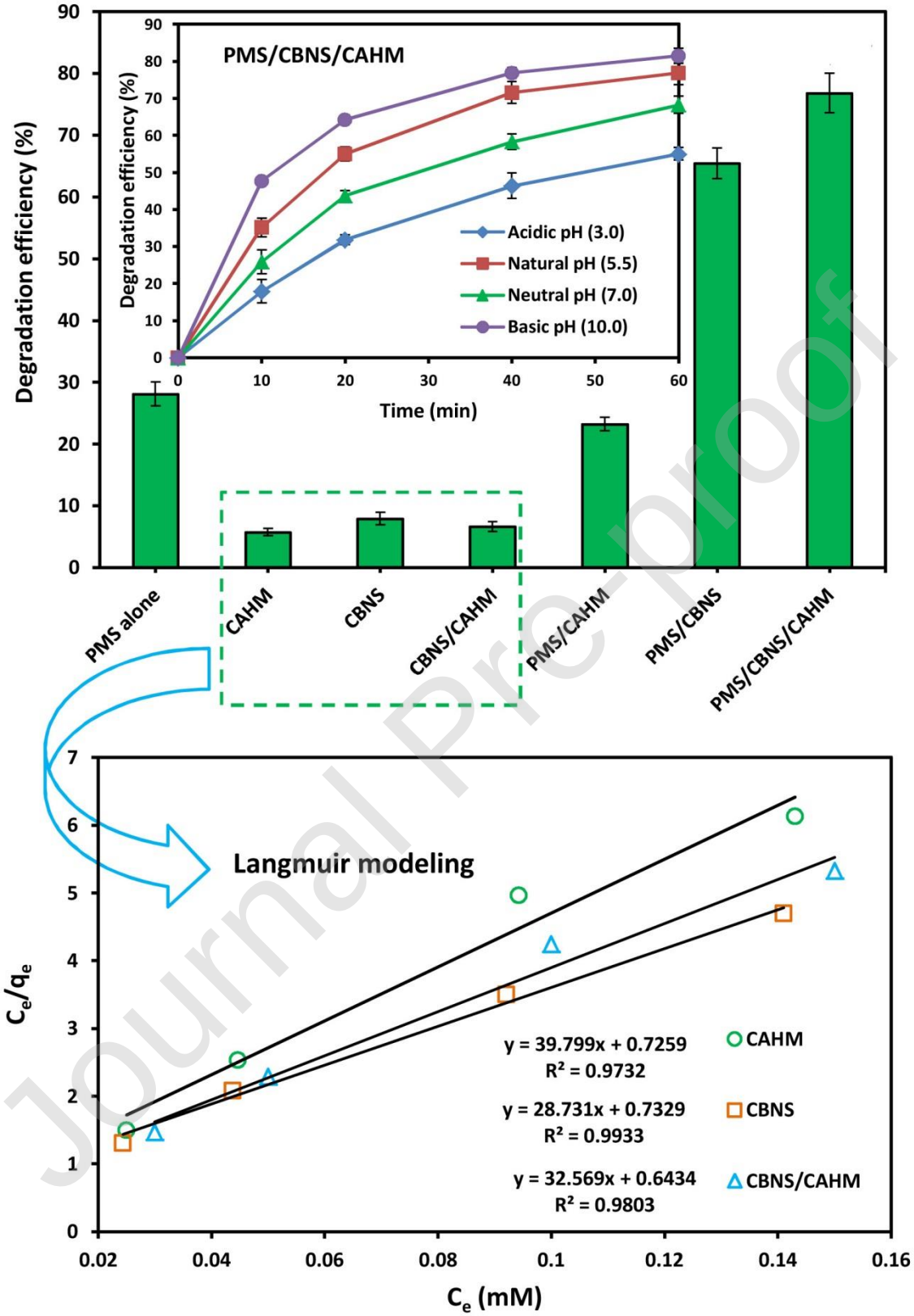

Fig. 4

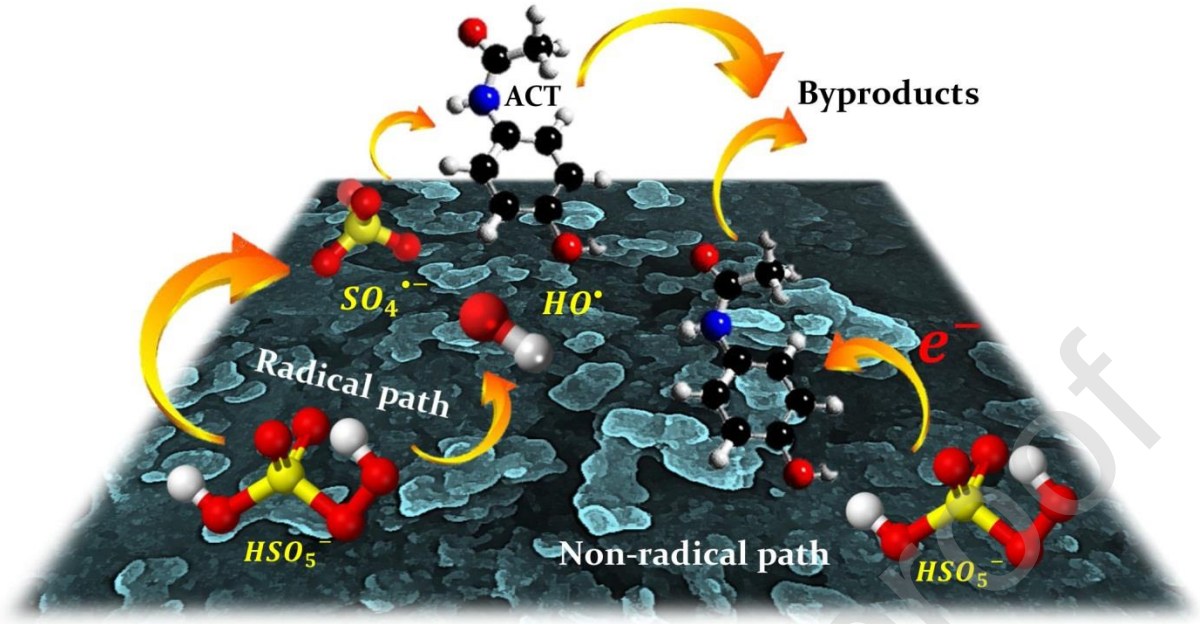

Fig. 5

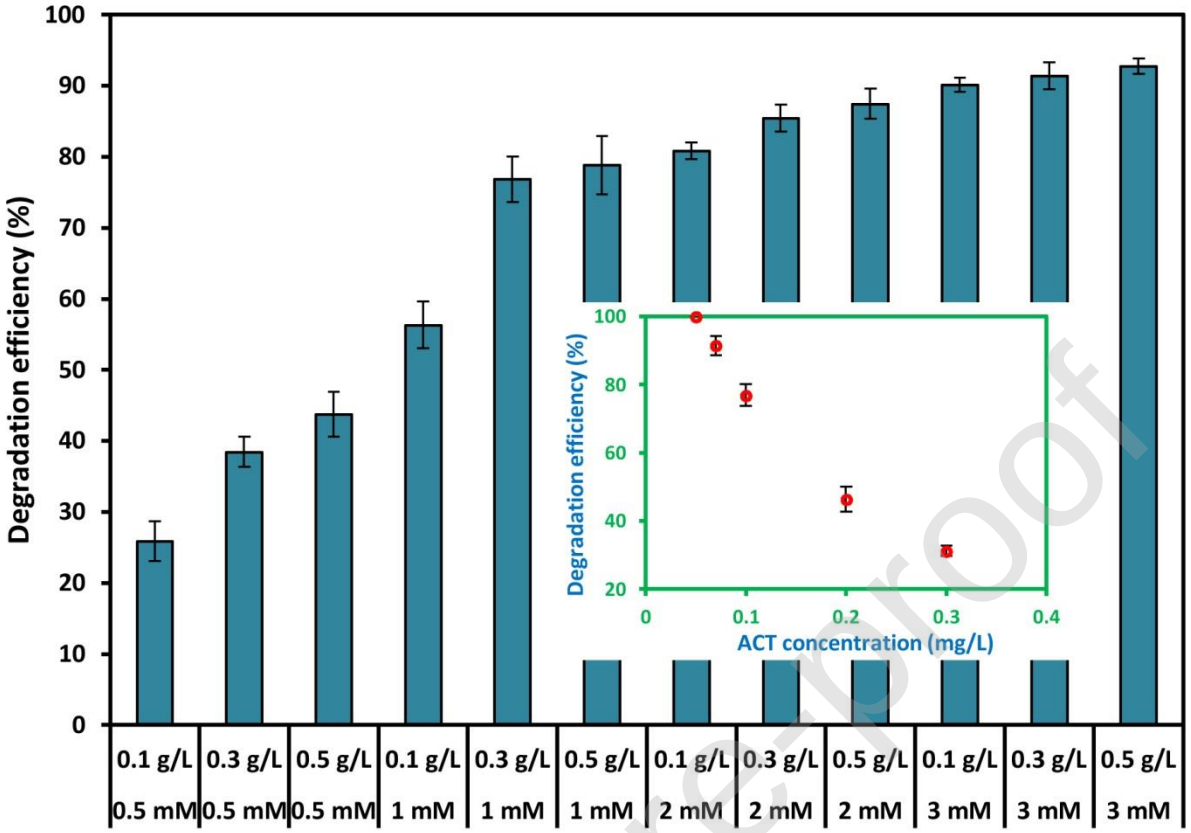

Fig. 6

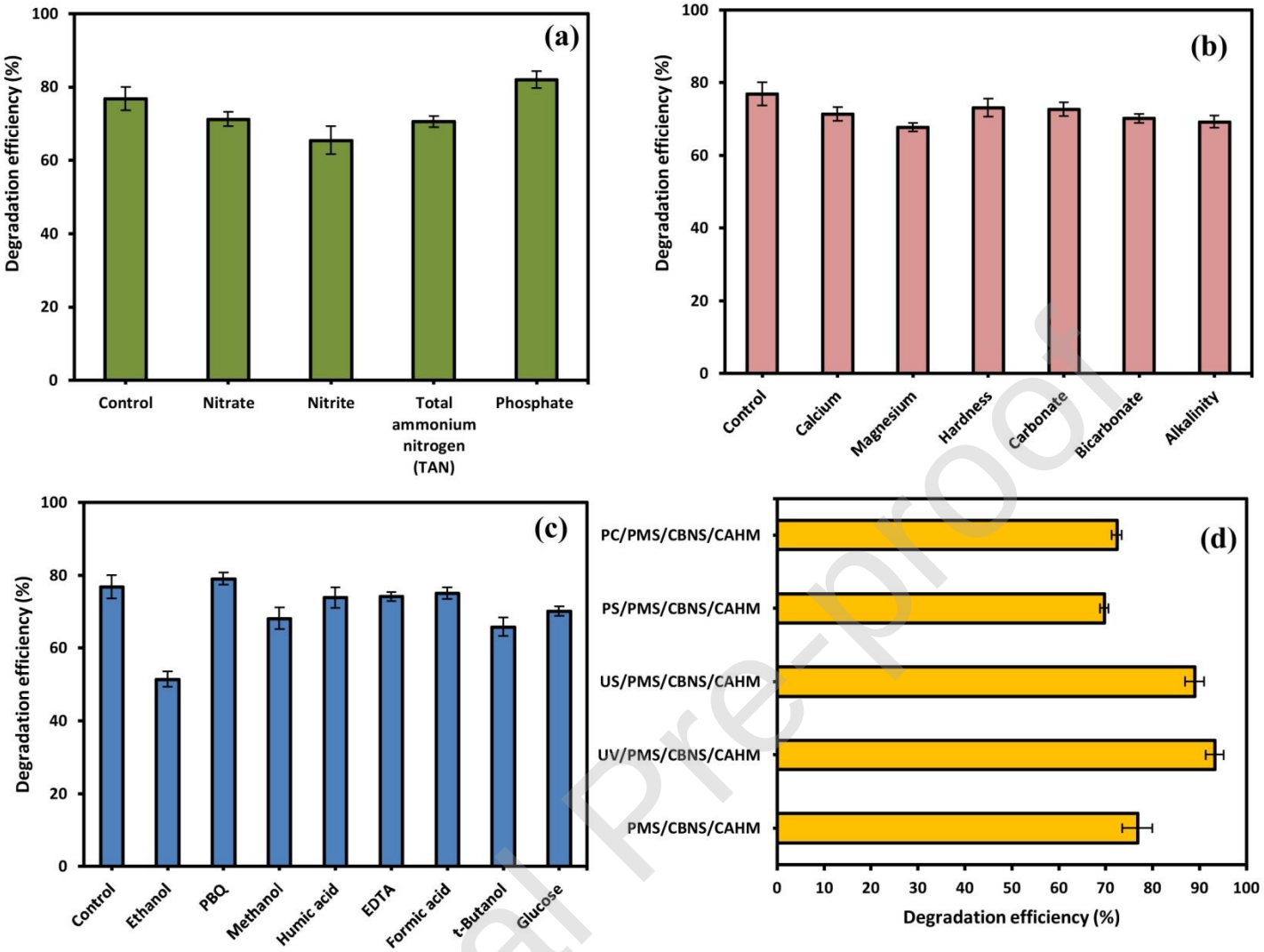

Fig. 7

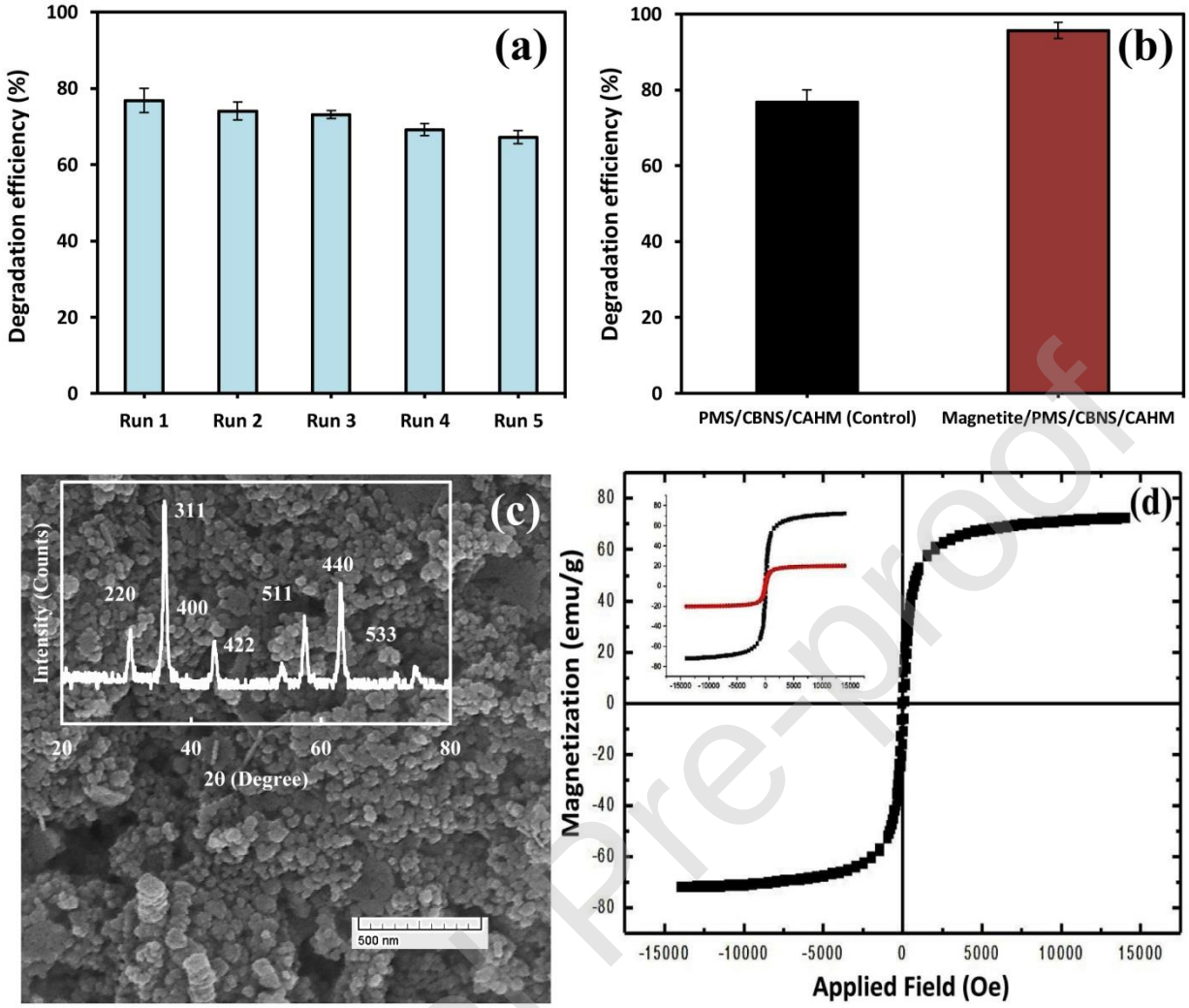

Fig. 8